Atmospheric Research 247 (2021) 105160

Contents lists available at ScienceDirect

Atmospheric Research

journal homepage: www.elsevier.com/locate/atmosres

Generation and enhancement mechanisms for extreme orographic rainfall associated with Typhoon Morakot (2009) over the Central Mountain Range of Taiwan

William Agyakwah[a,b], Yuh-Lang Lin[a,b,*]

[a] Department of Physics and Applied Science and Technology (AST) Ph.D., Program North Carolina A&T State University, USA
[b] Applied Science and Technology (AST) Ph.D., Program North Carolina A&T State University, USA

ARTICLE INFO

Keywords:
Typhoon Morakot (2009)
Tropical cyclone
Central Mountain Range
Orographic rain
WRF

ABSTRACT

The generation and enhancement mechanisms and essential ingredients for the extreme rainfall associated with Typhoon Morakot (2009) passing over Taiwan's Central Mountain Range (CMR) were investigated by using the Advanced Research Weather Research and Forecasting (WRF) model. First, we found that the extreme rainfall was due to the essential orographic rain ingredients: high precipitation efficiency, strong low-level jet, steep terrain, high moisture upstream, large convective system, and slower movement of the typhoon. Second, the Orographic Rain Index (ORI) proposed by Rostom (2015) was modified and tested by twelve (12) TC cases and found it has a good correlation with daily rainfall. Thus it can be used to help the prediction of extreme orographic TC rainfall. Third, we found there are two types of orographic rainfall mechanisms associated with Morakot, namely initiation and enhancement. These rainfall mechanisms may occur simultaneously at different locations, such as in northeast and southwest CMR. The orographic rain in the northeastern CMR was initiated by the high and steep CMR while the typhoon was still 200 km away. The rainfall was enhanced gradually and continually by the CMR when Morakot was approaching it, which produced a maximum rainfall of 265 mm/3 h starting at 1800 UTC August 7. The rain then decreased when the typhoon's eyewall structure and convection were damaged and weakened, respectively, when it invaded the high and steep CMR. Orographic rain was generated in the southwestern CMR initially when the conditionally unstable, southwesterly monsoonal flow impinged on the southern CMR. It was enhanced afterward by the merged monsoonal flow and Morakot's rainband leading to an extreme maximum rainfall of 311 mm/3 h starting 0000 UTC August 8. Later, this region of orographically enhanced TC rain moved northward along the western flank of the CMR. At last, we presented a conceptual model summarizing four key processes associated with the generation and enhancement of orographic TC rain over the southwest of CMR during the passage of typhoon Morakot (2009).

1. Introduction

Typhoon Morakot (2009) produced extreme rainfall over the northeast and southwest Central Mountain Range (CMR) of Taiwan during August 3–10, 2009. It started as a tropical depression and strengthened to become a tropical storm on August 4 until August 5. On 18 UTC August 5 (denoted as 8/5/18Z hereafter), it intensified to become Category 1 Typhoon Morakot at 8/8/00Z. Morakot reached its peak intensity early on August 7 with a low pressure of 945 hPa and sustained winds of 44 ms^{-1}, equivalent to a Category 2 hurricane. Later that day, Morakot made landfall in central Taiwan. About 24 h then, the storm moved off the west coast of the island and into the Taiwan Strait, where it turned north-northwestward (Digital Typhoon, 2019). From 8/8/00Z until 8/10/12Z, it weakened to become a tropical storm (NASA, 2009). Morakot produced extreme rainfall mainly in the mountains and the southwest plains of Taiwan during the period of 8/7/00Z to 8/10/00Z, 2009, which accumulated approximately 3000 mm in the southwestern CMR and 1623.5 mm/24 h in the Ali Mountains (e.g., Wu, 2013). This extreme rainfall event caused significant agricultural losses, estimated to be $494 million (USD), 673 deaths, and 26 people missing in Taiwan (Staff, 2009). Taiwan's CMR extends approximately from north-northwest to south-southeast with a length of about 270 km, a width of about 80 km, an average height of about 2.5 km, with the highest peak of 3952 m (FWM, 2019). Due to its high and steep mountains and isolation by oceans, the CMR plays a crucial role in deflecting typhoon tracks and modifying rainfall (e.g., Wang, 1980;

* Corresponding author at: 302H Gibbs Hall, North Carolina A&T State University, 1601 E. Market St., Greensboro, NC 27411, USA.
E-mail address: ylin@ncat.edu (Y.-L. Lin).

https://doi.org/10.1016/j.atmosres.2020.105160
Received 22 December 2019; Received in revised form 14 July 2020; Accepted 15 July 2020
Available online 26 July 2020
0169-8095/

Chang, 1982; Lin et al., 2005; Lin et al., 2016; see a review by Lin, 1993 and Lin, 2007).

It is well known that the amount and distribution of orographic tropical cyclone (TC) precipitation are strongly dependent on TC's synoptic environment during its passage over a mountain range (e.g., Lin, 2007; Purnell and Kirshbaum, 2018). One way to help understand the orographic influence on rainfall is to take the ingredient approach, such as in Lin et al. (2001), which extended Doswell et al.'s (1996) ingredient argument, in which the orographic precipitation (P) is determined by the following equation:

$$P = \varepsilon\left(\frac{\rho_a}{\rho_w}\right)(\boldsymbol{V}_H \cdot \nabla h + w_{env})\left(\frac{L_s}{c_s}\right)q_v, \quad (1)$$

where ρ_w and ρ are the liquid water density and air density, respectively, ε is the precipitation efficiency, w_{oro} and w_{env} are the vertical velocity forced by orography and environment, respectively, q_v is the water vapor mixing ratio, L_s and c_s are the horizontal scale of the precipitating system and its moving speed, respectively. Based on Eq. (1), heavy orographic precipitation requires any combination of the following ingredients: (1) high precipitation efficiency (ε), (2) strong orographic lifting (w_{oro}) or Low Level Jet (LLJ) (U) and a steep mountain ($\partial h/\partial x$) since $w_{oro} = U\,\partial h/\partial x$, (3) strong environmental lifting (w_{env}) (e.g., the release of conditional instability-large CAPE, potential instability, low-level convergence, upper-level divergence, etc.), (4) large moist airflow upstream (q_v), (5) large preexisting convective system (L_s), and (6) slow translational motion of the storm (c_s). Studies have shown that several heavy orographic rainfall cases that occurred during the passage of typhoons over Taiwan's CMR are closely related to some common ingredients (e.g., Chiao and Lin, 2003; Yang and Ching, 2005; Witcraft et al., 2005; Yang et al., 2008; Huang and Lin, 2014 (hereafter referred to as HL14); also see Lin, 2007 for a review).

Based on the ingredient approach and numerically simulated Tropical Storm (TS) Rachel (1999) over Taiwan, Chiao and Lin (2003) attributed the first spell of heavy orographic rainfall to the intensification of southwesterly monsoon current and strong LLJ over the southwest CMR. And the second spell of heavy rainfall to the orographic lifting of the LLJ merged TS Rachel's rainbands and southwesterly monsoonal flow. In investigating factors leading to heavy rainfall associated with Supertyphoon Bilis (2000), Witcraft et al. (2005) found that the essential ingredients are: high CAPE, potentially unstable air layer, very moist airflow impinging on the CMR, and an LLJ associated with the typhoon's outer circulation. In studying extreme rainfall associated with typhoons passing over the CMR, HL14 showed that the abundant water vapor, slow translation speed, and strong orographic lifting are three major common ingredients for extreme orographic rainfall associated with the landfall of Typhoon Morakot (2009) on Taiwan's CMR, with the abundant water vapor playing an important role. Rostom (2015) also examined the common ingredients for heavy rainfall associated with the passage of Hurricanes Hugo (1989) and Isabel (2003) over the Appalachian Mountains. It was found that the major common ingredients were: high precipitation efficiency, strong LLJ, strong orographic lifting, a concave geometry, high moist upstream, large preexisting convective system, and slow translational motion of the storm. Besides, it is found that conditional and potential instabilities played minor roles in producing heavy rainfall associated with Hugo and Isabel.

For the extreme rainfall associated with Typhoon Morakot (2009), several other previous studies found the following factors were responsible: (a) convective cells embedded in Morakot's eyewall and rainbands, (b) abundant moisture associated with monsoonal flow, (c) convergence of the southwesterly monsoonal flow and typhoon circulation, (d) orographic lifting by the CMR and, and (e) slow translation speed (e.g., Ge et al., 2010; Hong et al., 2010; Lin et al., 2011; Tao et al., 2011; Wu et al., 2011; Yu and Cheng, 2013; HL14). Factors (b) – (e) are a subset of the common ingredients inferred from Eq. (1) as discussed above. In (a), it remains unclear whether the extreme accumulated rainfall occurred in the northeast (NE) and southwest (SW) of the CMR was caused by the enhancement of the preexisting convective cells embedded in the eyewall or rainbands associated with Morakot or a moist airstream with no preexisting convective cells. Thus, it is necessary to understand these mechanisms, including their relative importance, in producing the extreme rainfall in the NE of the CMR.

In this study, we will use the Advanced Research Weather Research and Forecasting (WRF) model to examine the generation and enhancement mechanisms and the essential ingredients responsible for the extreme orographic TC rain associated with Typhoon Morakot (2009) at the NE and SW of the CMR. The goal of this study is to improve the understanding of the basic dynamics and physics of heavy orographic precipitation and improve its prediction. We will discuss the model description and experimental design in section 2, which includes the verification of the Best case simulation. We will examine the essential ingredients for orographic rain associated with Typhoon Morakot (2009) in section 3. Investigate the relative importance of generation and enhancement mechanisms on the production of extreme rainfall associated with Morakot in the SW and NE of the CMR in section 4. And finally, present the concluding remarks in section 5.

2. Methodology

2.1. Model description

The WRF model version 3.3.1 (Skamarock et al., 2008) was adopted for the numerical simulations of Typhoon Morakot (2009) and its associated rainfall over Taiwan's CMR. The WRF model is a numerical weather prediction system developed to help with a better understanding of mesoscale weather by incorporating initial idealized data or better forecasting weather operationally by incorporating initial real data into the model. The WRF model is a three-dimensional, non-hydrostatic, fully compressible model using terrain-following vertical coordinates with stretched grid resolution, one-way or two-way multiple-nesting capability, options for upper and lateral boundary conditions, etc. The WRF model governing equations are written in flux-form with conserved mass and dry entropy.

The WRF model provides a flexible and robust platform for operational forecasting, while also offering more options in advanced schemes in physics parameterizations and numerical methods, including data assimilation techniques.

2.2. Experimental design

Three domains with resolutions of 27 km (D1), 9 km (D2), and 3 km (D3) and nested grid two-way interactions at 9 km and 3 km, were used for this study as shown in Fig. 1. Vertically, there are 28 stretched sigma levels for all the nested domains with the top at about 50 hPa and a higher resolution in the lower troposphere, especially the planetary boundary layer. The time step intervals are 150, 50, and 16.7 s for domains D1, D2, and D3, respectively. All simulations of the three domains in the study start at 8/3/00Z and end at 8/10/00Z. The physics parameterization options used in the simulations include Goddard microphysics scheme (Tao et al., 1989) that was modified from Lin et al. (1983), Kain-Fritsch cumulus scheme (Kain, 2004), Rapid Radiative Transfer Model longwave radiation physics scheme (Mlawer et al., 1997), Dudhia shortwave radiation scheme (Dudhia, 1989), and Yonsei University scheme of the planetary boundary layer (Hong et al., 2006).

The cumulus parameterization scheme was activated in all nested domains to avoid energy accumulation at grid points, especially in the inner domain (D3). The National Centers for Environmental Prediction (NCEP) Global Forecast System data of 1° resolution at 8/03/00Z was used as initial and boundary conditions. The NCEP daily high-resolution real-time global sea surface temperature analysis data of 0.5° resolution was used to update the SST every 6 h during the time

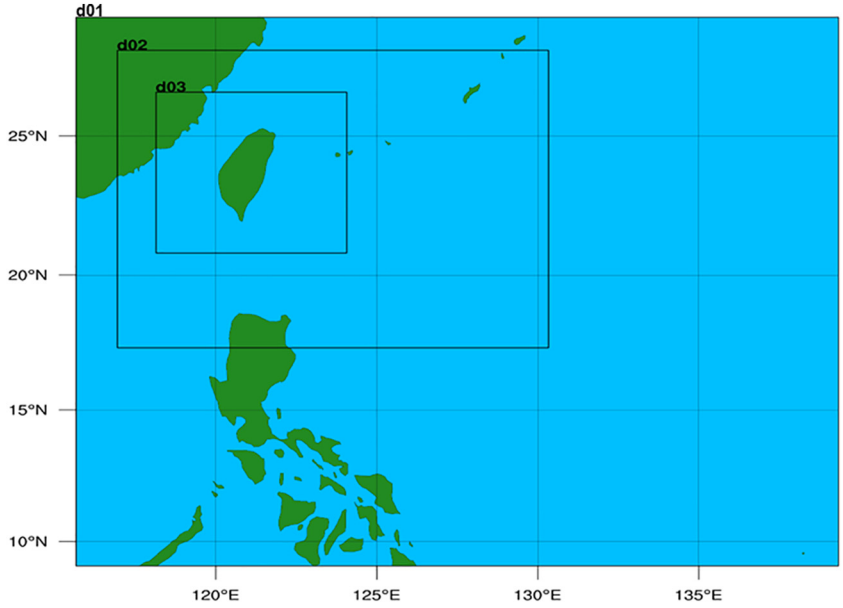

Fig. 1. Domain configuration for Typhoon Morakot simulations with three domains of 27 km (D1, i.e. d01), 9 km (D2, i.e. d02), and 3 km (D3, i.e. d03) grid resolutions.

integrations. We generated the model TC through the initial data and associated environmental conditions; thus, there is no bogus vortex initialization employed in the initial data. Japan Meteorological Agency (JMA) best track data (Digital Typhoon, 2019) was used to verify and discuss the relevant factors that led to extremely heavy precipitation.

In this study, there are five (5) simulated cases. The NCEP Final Operational Global Analysis Data (hereafter referred to as the FNL data) was used to initialize two of them with one starting at 8/2/12Z (Case F02) and the other starting at 8/03/00Z (Case F03). Both of them end at 8/10/00Z. The European Centre for Medium-Range Weather Forecasts *Re*-Analysis data (hereafter referred to as ERA data) was used to initialize the other three cases with starting times 8/2/12Z (Case E02), 8/3/00Z (Case E03) and no terrain (NT) case with starting time at 8/3/00Z. Similar to F02 and F03 cases, the E02, E03, and NT cases ended at 8/10/00Z. The NT case was initialized with ERA because the selected Best case simulation was E03, which will be discussed further in subsection 2.3. The purpose of the NT case was to investigate the impact of orography on precipitation enhancement. As for cases F02 and F03, Cases E02, E03, and NT end at 8/10/00Z. These cases were run with the idea to have a good track forecast since it is significant in predicting an accurate quantitative precipitation forecast (Xie and Zhang, 2012).

2.3. Verification of the best case simulation

Verification of the simulated Typhoon Morakot (2009) includes track, intensity, reflectivity, and precipitation. In comparing the tracks of cases E02, E03, F02, F03, and NT with the best track data at the initial observed time (8/6/12Z), E02, E03, and NT cases move faster than the observed while cases F02 and F03 lag behind. Later on, E03 and NT cases mimic the best track comparatively well, and case E03 moves southward while case NT moves northward. On 8/8/00Z, the F02, F03, and NT cases lag, and the E03 case follows the best track data with less track error compared to the other cases. And for the E02 case, the TC is lost after 8/7/12Z. From Table 1, case E03 had the least overall average track error of 42.4 km. Based on the simulated tracks of these cases, we found that case E03, in which the WRF simulation was initialized with ERA data starting at 8/03/00Z and ending at 8/10/00Z, compared the best with the JMA best track of Typhoon Morakot (Fig. 2). Thus, case E03 was chosen as the Best case simulation for further analysis to study the formation mechanisms of orographic rain

Table 1
Assessment of Track error (km) for various cases.

Date	E02	E03 (Best Case)	F02	F03	NT
6/12Z	184	62	99	106	70
7/00Z	129	47	146	109	26
7/12Z	158	35	115	86	30
8/00Z	NA	45	142	142	61
8/12Z	NA	23	92	13	67
Average	157	**42.4**	118.8	91.2	50.8

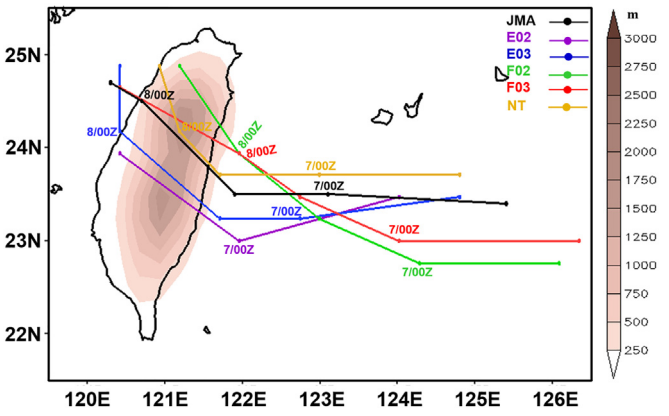

Fig. 2. Observed (black), E02 (purple), E03 (blue), F02 (green), F03 (red) and NT (brown) tracks of Typhoon Morakot (2009) from 8/6/12Z to 8/8/12Z.

associated with the passage of Typhoon Morakot (2009) over the CMR. The WRF simulated Morakot in the Best case made landfall in Central Taiwan on August 7, the same as the observed track. Generally speaking, the simulated track compared well with the JMA best track.

The WRF simulated maximum wind speed (V_{max}) was compared with the JMA's best track (Fig. 3a). With an emphasis on the Best case simulation, the WRF simulated V_{max} showed a relatively slow spin-up during the first two days, then greater intensity in the remaining five days. The WRF simulation had a V_{max} of 42 ms^{-1}, which is slightly greater than V_{max} of 38 ms^{-1} observed in JMA's best track. In comparing their minimum sea level pressure (MSLP), the WRF simulated

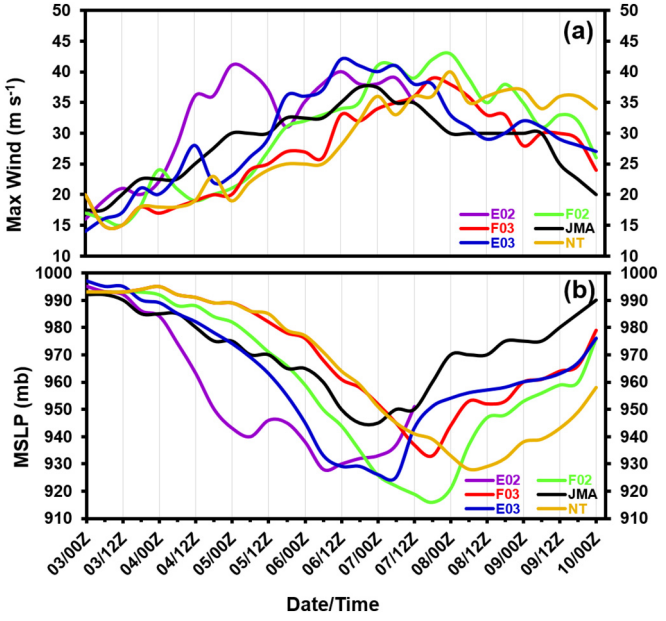

Fig. 3. Typhoon Morakot (2009) (a) maximum wind speed (ms^{-1}) and (b) mean sea level pressure (hPa) from 8/3/00Z – 8/10/00Z.

intensity is weaker than that of the JMA's best track in the first two days and stronger in the last five days. WRF recorded the lowest MSLP of 925 hPa, and JMA recorded 945 hPa (Fig. 3b). In general, the simulation correctly mimics the track, which, in turn, produced accurate rainfall patterns despite the overprediction.

The 3-km resolution simulated composite reflectivity and accumulated precipitation were compared with observed composite reflectivity and accumulated precipitation, respectively, to verify the accuracy of the simulated data. We used the 3-km resolution simulated data because it has a finer resolution, which can provide more details. In Fig. 4, the observed composite reflectivity is compared with the simulated composite reflectivity from 8/7/00Z to 8/8/18Z. It shows high reflectivity in the South China Sea (south of Taiwan), especially from 8/7/00Z to 8/8/06Z. The WRF simulation has a similar phenomenon with a relatively higher intensity than the observed. The observed composite reflectivity is intense in the South China Sea, the eyewall region, and the northern part of the CMR during 8/7/00Z. The WRF simulation also displays a similar phenomenon with a relatively higher intensity in the eyewall region. The eyewall region showed higher intensity until landfall time around 8/7/12Z; the maximum intensity shifted to the outer rainband region. This incident could be a result of the collapse of the eyewall, which reduced the strength of the typhoon. After landfall, the rainband reflectivity showed maximum intensity primarily in the southern region of Taiwan's CMR. The TC moved northwest, and this caused the maximum reflectivity to move poleward, which led to maximum intensity in the middle and north of the CMR. The WRF simulation has higher intensity and speed of motion. In general, the composite reflectivity of the simulated data compared well with the observation.

Also, we compared the observed accumulated rainfall with the simulated rainfall during the period 8/7/16Z – 8/8/16Z (8/8/00 LST – 8/9/00 LST) for the following cases: Best case (E03), F02, F03, and NT (Fig. 5a). For case E02, it was exempted because the TC was lost after 8/7/12Z (Fig. 2). Since the precipitation is sensitive to the typhoon location and intensity, we compared the accumulated rainfall in different periods in which the typhoon is at the same locations in different cases. Thus, the observation at the period 8/7/16Z – 8/8/16Z (8/8/00 LST – 8/9/00 LST) was compared with the simulated cases at the periods: (i) Best case (E03) 8/7/16Z – 8/8/16Z (8/8/00 LST – 8/9/00 LST) (ii) F02 case 8/8/07Z – 8/9/07Z (8/8/15 LST – 8/9/15 LST), (iii) F03 case 8/8/04Z – 8/9/04Z (8/8/12 LST – 8/9/12 LST) and (iv) NT case 8/7/22Z – 8/8/22Z (8/8/06 LST – 8/9/06 LST) (LST = UTC + 8 h). We chose the period 8/7/16Z – 8/8/16Z (8/8/00 LST – 8/9/00 LST) because a massive amount of rainfall was recorded in that period. In this period, the observed and the simulated cases, except the NT case, all have a vast amount of rainfall occurring at the southern sector along the CMR. The NT case had the least maximum rainfall, which could be attributed to the absence of the high and steep CMR playing a significant role in enhancing the TC rainfall through the process of orographic lifting. The WRF simulated maximum rainfall for the Best case (E03), F02, F03, and NT cases are 2024 mm, 1677 mm, 1390 mm, and 486 mm, respectively. The Best case (E03) simulation overpredicted the observed rainfall data of 1402 mm. Despite the overprediction of rainfall by this simulation, the rainfall pattern looks almost the same as the observed rainfall data. And is evidenced by comparing the 3 h accumulated rainfall of WRF-simulated Best case (E03) and observed rainfall data from the Alishan weather station (23.30°N, 120.48°E) during the event of Typhoon Morakot (2009) from 8/5/01Z to 8/9/22Z (Fig. 5b). From the time series plot, the observed rainfall pattern is well captured by the simulated rainfall. This complements the numerous studies on Typhoon Morakot by accurately producing the rainfall pattern, which is a challenging predictability problem. For example, in Nguyen and Chen (2011), the precipitation pattern of simulations with different initializations for Typhoon Morakot had numerous different rainfall patterns from observations. Generally speaking, comparing the observed typhoon track, maximum wind speed, MSLP, composite reflectivity data, and observed rainfall data, the simulated results compared well. Due to that, it assures us to use the simulated results to examine the essential orographic rain ingredients, as well as the generation and enhancement mechanisms related to Typhoon Morakot (2009).

3. Common ingredients for extreme orographic TC rain

As discussed in the Introduction, Lin et al. (2001) applied Doswell et al. (1996) ingredient approach to the upslope orographic precipitation problem. Note that $V_H \cdot \nabla h$ (refer from Eq. (1)) represents the orographically forced upward motion, i.e. w_{oro}. In Lin et al. (2001) study, they used common synoptic and mesoscale environmental features favorable to heavy orographic rainfall in the United States. They examined whether these features are present in the European Alps, Taiwan, and Japan. The results showed the following synoptic and mesoscale features were present: 1) conditionally or potentially unstable airflow, 2) very moist low-level jet, 3) steep terrain and 4) a quasi-stationary system which impedes the motion of the convective system over the affected area. Lin (2007), identified that the occurrence of heavy orographic precipitation needs any combination of the following ingredients: (1) high precipitation efficiency (ε), (2) strong orographic lifting (w_{oro}) or LLJ (U) and a steep mountain ($\partial h/\partial x$) since $w_{oro} = U\,\partial h/\partial x$, (3) strong environmental lifting (w_{env}) (e.g., release of conditional instability – large CAPE, potential instability, low-level convergence, upper-level divergence, etc.), (4) large moist airflow upstream (q_v), (5) large preexisting convective system (L_s), and (6) slow translational motion of the storm (c_s).

In this study, we examined the common ingredients using the WRF model to help understand the basic dynamics and physics of heavy TC orographic precipitation and improve its prediction. The ingredient to be examined first was precipitation efficiency, which is the ratio of total precipitation to the total available moisture of a convective system (Lin, 2007). Previous studies showed several factors such as the advection of hydrometeors, evaporation associated with rainfall below the cloud base, entrainment rate of environmental air into the cloud, and environmental shear might contribute to precipitation efficiency (Fankhauser, 1988). Fig. 6 shows the precipitation efficiency of a selected area (111 km × 56 km) averaged from 8/8/00Z to 8/9/00Z. We chose this area and date because the largest accumulated rainfall

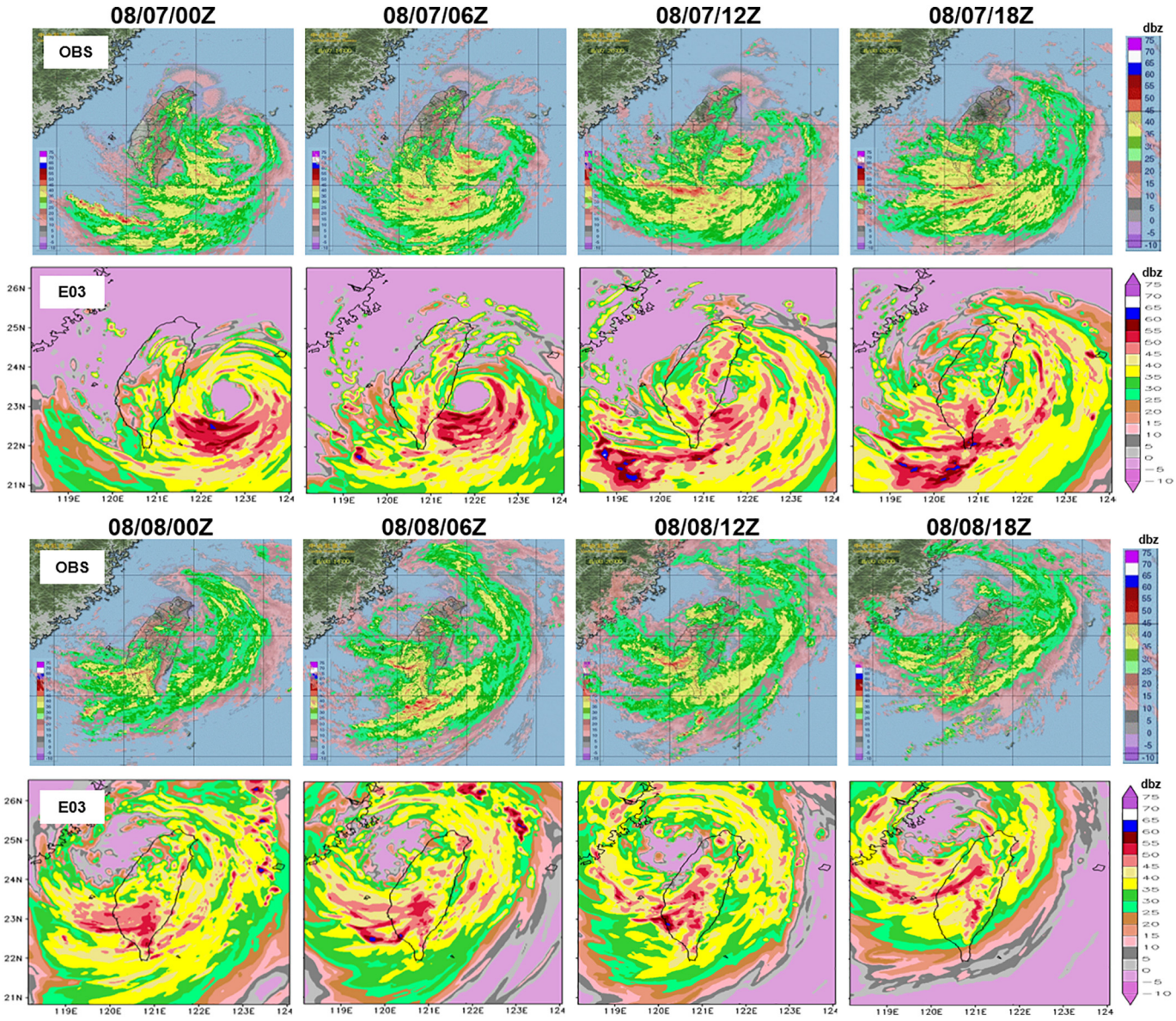

Fig. 4. Composite Reflectivity of Typhoon Morakot from 8/7/00Z to 8/8/18Z for (a) observed (OBS) field from the Doppler radar network in Taiwan and (b) WRF simulated E03 (Best) case radar echo field.

occurred in this area during that period. The WRF simulated precipitation efficiency is 91%, which was estimated by dividing the averaged total precipitation (626 mm) (Fig. 6a) by the vertically integrated available moisture (690 mm) (Fig. 6b) in the selected area. This shows the precipitation efficiency associated with WRF simulated Morakot is high. The second ingredient examined is whether there is an LLJ. An LLJ is a jet stream that is typically found in the lower 2–3 km of the troposphere (AMS, 2018). Fig. 7a shows the 10 m wind at 8/8/00Z with a maximum LLJ of 35 ms^{-1} and an average of 25 ms^{-1}, which is strong enough to produce substantial orographic lifting (w_{oro}) when the low-level airstream impinges on Taiwan's CMR. Steep orography (large ∇h) is the third ingredient examined. It is estimated by using the mountain slope represented in the 3-km grid resolution. The slope of the selected area is ~0.088 (that is 2.3 km/26 km) and it can be considered as being steep. The fourth ingredient examined is suitable mountain shape (e.g. concave) for the converging flow field (or say, large $w_{oro} \propto V_H \cdot \nabla h$). For flow over a mountain range, the low-level upward motion is induced by either orography or the environment (Lin, 2007) as:

$$w = w_{oro} + w_{env} \tag{2}$$

As discussed in Lin et al. (2001) and Lin (2007), for simplicity, the vertical motion is split linearly into environmentally (w_{env}) and orographically (w_{oro}) induced vertical motions. The orographically forced upward vertical motion can be estimated approximately by the lower boundary condition for flow over mountains given as:

$$w_{oro} = \frac{Dh}{Dt} \approx V_H \bullet \nabla h \tag{3}$$

where $h(x, y)$ is the mountain elevation as a function of x and y, and V_H is the low-level horizontal wind velocity. The environmentally forced upward vertical motion (w_{env}) may be induced by, for example, the release of conditional instability, low-level convergence, etc. with a strong LLJ and steep orography (from earlier two ingredients), it may result in strengthening the w_{oro}. Also, the selected area of the CMR has a concave geometry (Fig. 7a), which assisted in the generation of confluent flow and enhanced upward motion, as proven by other studies on heavy orographic rain (e.g., Chiao and Lin, 2003; Witcraft et al., 2005).

The fifth ingredient examined is w_{env}. The w_{env} is determined by the combination of factors like a release of conditional instability, potential

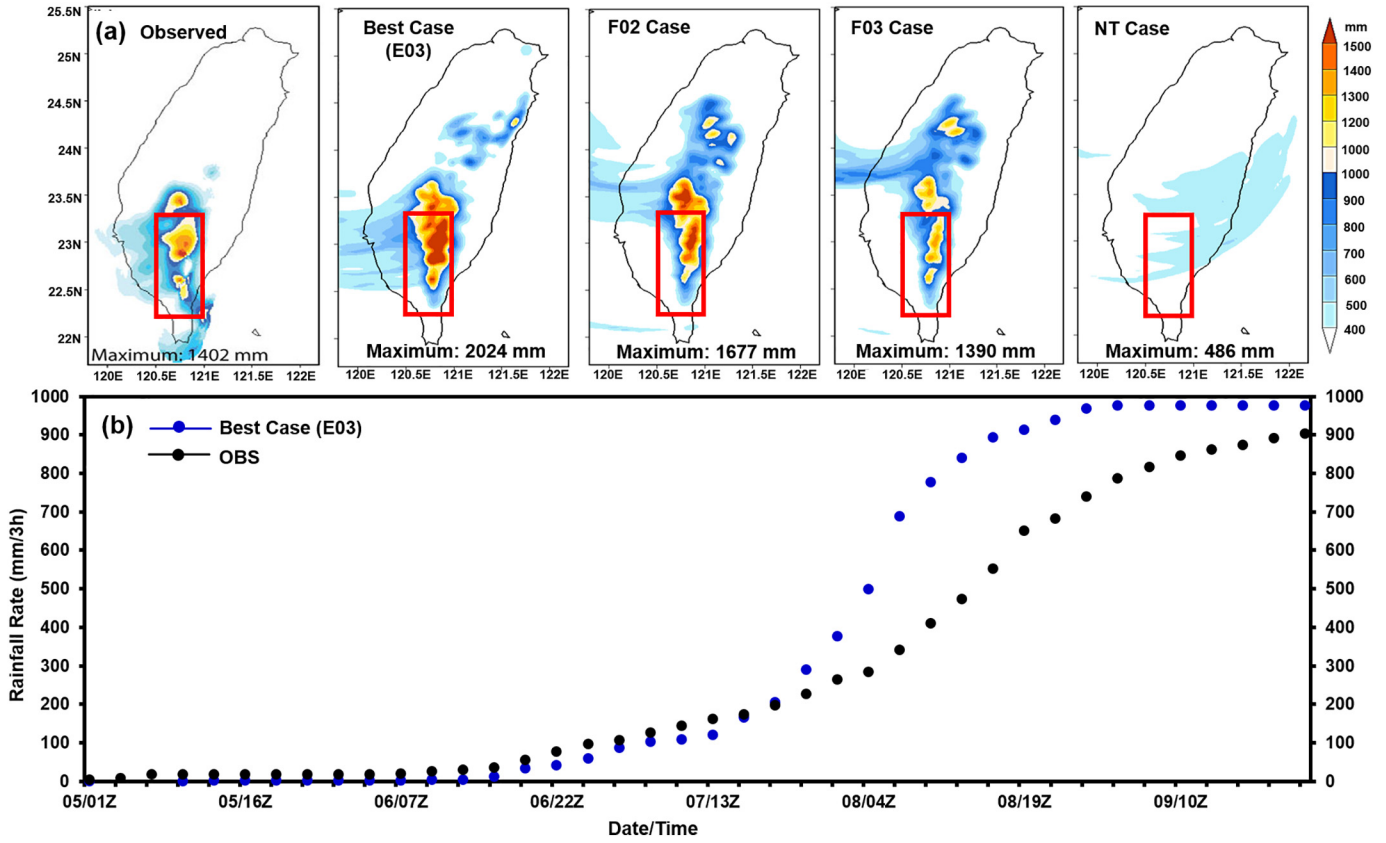

Fig. 5. (a) Comparison of 24 h accumulated rainfall of observation for the period 8/7/16Z – 8/8/16Z (8/8/00 LST – 8/9/00 LST) with the simulated cases in different periods when the typhoon is at the same location in case: Best case (E03) 8/7/16Z – 8/8/16Z (8/8/00 LST – 8/9/00 LST), F02 case 8/8/07Z – 8/9/07Z (8/8/15 LST – 8/9/15 LST), F03 case 8/8/04Z – 8/9/04Z (8/8/12 LST – 8/9/12 LST) and NT case 8/7/22Z – 8/8/22Z (8/8/06 LST – 8/9/06 LST) (LST = UTC + 8) (b) Comparison of 3 h accumulated rainfall of WRF simulated E03 (Best) case and observed rainfall data from Alishan weather station (23.30°N, 120.48°E) during the event of Typhoon Morakot (2009) (8/5/01Z – 8/9/22Z). (Adapted after Huang and Lin, 2014).

instability, low-level convergence, and upper-level divergence, which can be approximately estimated from Eq. (3) as w-w_{oro}. A conditionally or potentially unstable airflow upstream is the sixth ingredient examined. The averaged and maximum CAPE over the selected area was 48 J kg^{-1} and 248 J kg^{-1}, respectively (Fig. 7b). This implies that the release of conditional instability plays a minor contribution in generating strong updraft (w_{env}), leading to heavy orographic rain. We accessed the potential instability by examining the 24 h simulated surface-850 hPa $\partial\theta_e/\partial z$ for the selected area (Fig. 7c). Since there existed no negative values ($\frac{\partial\theta_e}{\partial z} > 0$) in these areas, which means the atmosphere was potentially stable. This implies potential instability played an insignificant role in the formation of heavy orographic rainfall associated with Typhoon Morakot. The seventh ingredient examined was upstream moisture content. The upstream water vapor

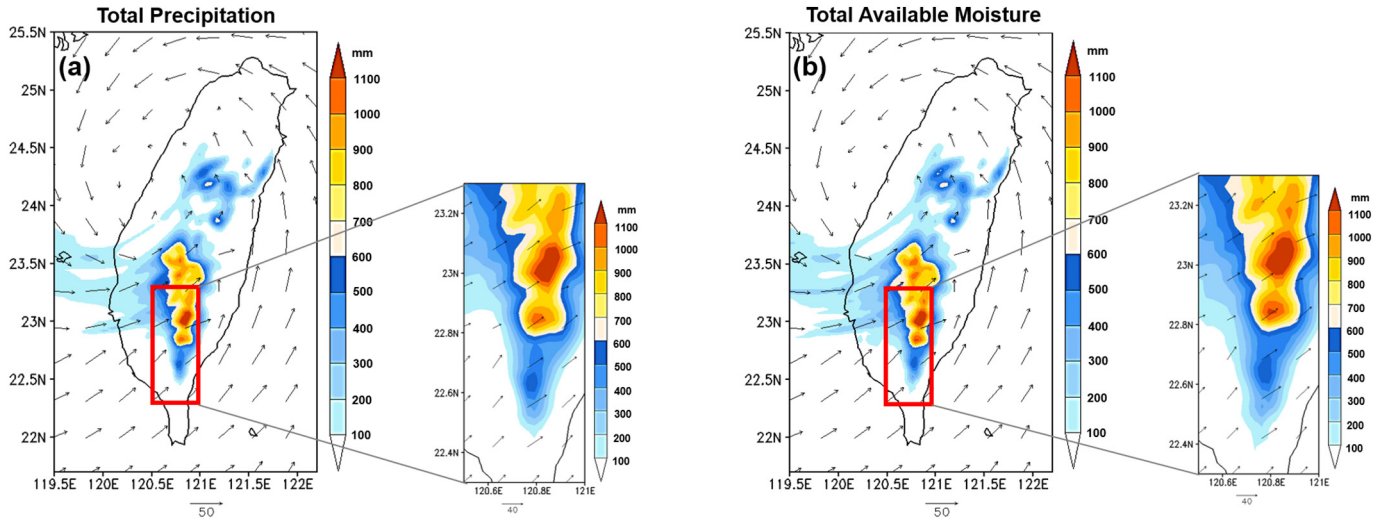

Fig. 6. WRF simulated Best case (E03) precipitation efficiency of the selected area (111 km × 56 km), which is averaged from 8/8/00Z - 8/9/00Z using (a) total precipitation and (b) vertically integrated available moisture. The wind field is at 8/8/00Z.

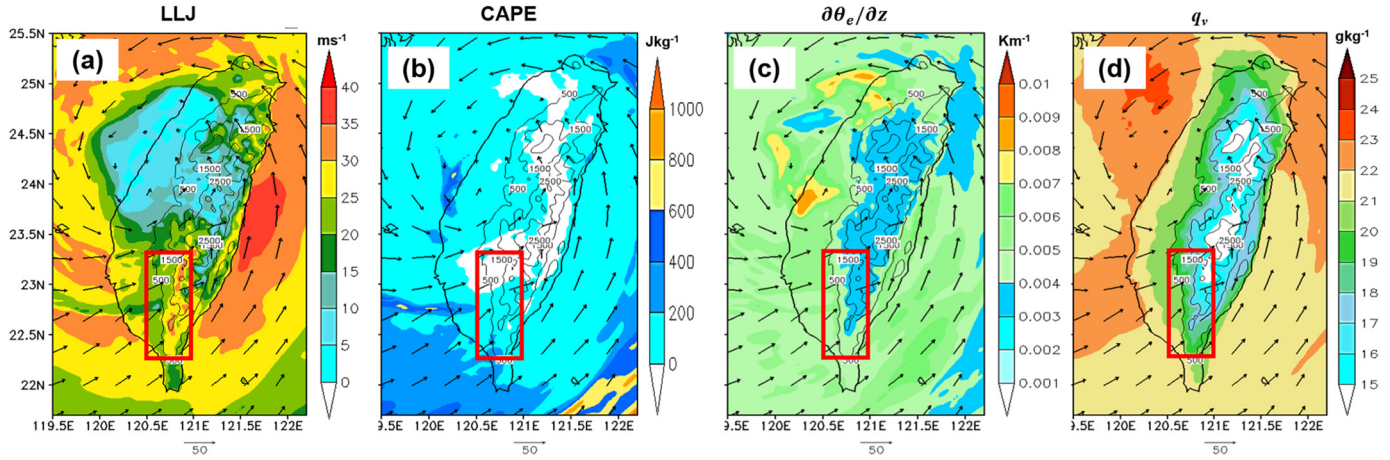

Fig. 7. Examining some of the common ingredients for extreme orographic TC rain using the WRF simulated Best case (E03), which includes: (a) Low-level jet winds (10 m level) (shaded; ms^{-1}) at 8/8/00Z. 24 h (8/8/00Z - 8/9/00Z) averaged (b) CAPE from the surface to 850 hPa (c) potential instability ($\partial\theta_e/\partial z$) from the surface to 850 hPa and (d) water vapor mixing ratio (q_v). The wind field is at 8/8/00Z, and the contour lines are terrain height with an interval of 1000 m.

mixing ratio (q_v) was used to investigate this property. The q_v over the selected area had an averaged, and maximum values of 19 g kg^{-1} and 22 g kg^{-1}, respectively, and the highest moisture was seen around the outer rainband region of the typhoon (Fig. 7d). Based on this result, the q_v over the selected area has a high moisture content upstream; hence it was preferable for heavy orographic rainfall. The eighth ingredient examined was the size of the Morakot. Using the simulated composite reflectivity and observed radar imagery (Fig. 4), Typhoon Morakot has an L_s of about 300 km in diameter, which is large enough to help produce heavy rainfall. The ninth ingredient examined was the moving speed of the Morakot. It had an average speed of 5 ms^{-1}, which is slow enough compared with other typhoons, which passed over the CMR to help produce heavy orographic rainfall (HL14).

From the above analysis and discussion, the essential ingredients which were responsible for the heavy orographic rainfall produced by Typhoon Morakot were eight: high precipitation efficiency of the incoming airstream, strong low-level jet, steep orography, favorable mountain geometry, strong orographically induced vertical motions, high moisture upstream, large convective system and slow movement of the convective system. In terms of essential ingredients for heavy TC orographic rainfall, this study is consistent with other previous studies on Typhoon Morakot (e.g., Hong et al., 2010; Yen et al., 2011; Chien and Kuo, 2011; Lin et al., 2011; Wu et al., 2011; HL14), but more complete. One ingredient that differs from what was found in Witcraft et al. (2005) is that CAPE is not an essential ingredient for orographic rainfall in the case of Morakot.

Based on the essential common ingredients for orographic TC rain, Rostom (2015) proposed ORI, i.e., V_n (dh/dn) (L_s/c_s) (RH), where V_n is the normal component of the incoming wind to the steepness of the local mountain range (dh/dn), L_s and c_s are the size and speed of the storm, respectively, and RH is the relative humidity. This ORI is modified to be V_n (dh/dn) (L_s/c_s) q_v, where q_v is the water vapor mixing ratio. In this way, the ORI is not temperature-dependent, unlike using RH. We tested this modified ORI by using the following historical TC cases: Hurricanes Hugo (1989) and Isabel (2003) from Rostom (2015); Supertyphoon Bilis (2000) from Witcraft et al. (2005); Typhoon Toraji (2001) from Yang and Ching (2005); and Typhoons Krosa (2007), Sepat (2007), Sinlaku (2008), Jangmi (2008), Fung-Wong (2008), Morakot (2009), Fanapi (2010) and Saola (2012) from HL14. The results are shown in Table 2 with approximate estimates of the essential common orographic ingredients, which gave a good correlation of 0.7 with the daily rainfall (Fig. 8a), and it compared well with ORI estimated by Rostom (2015) (Fig. 8b). Thus the modified ORI can help the prediction of extreme orographic TC rainfall. For example, Typhoon Morakot (2009) comparatively had the highest rainfall rate of 1402 mm day^{-1} and concurrently had the highest ORI of 21.4. The remarkable features of Typhoon Morakot event were that, among the ingredients mentioned above, 1) it had strong orographic lifting caused by the steep mountain, 2) slowest moving speed, 3) abundant water vapor content, and 4) the TC moving speed was the dominant factor, as pointed out by HL14. This means the moving speed of TC has the strongest relationship with the heavy orographic rainfall of these four.

4. Relative importance of generation and enhancement mechanisms for orographic TC rain

As discussed in the introduction, this section investigates the relative importance of orographic rain generation and enhancement. We observed the evolution of Morakot using rain rate (mm/3 h) from 8/7/00Z to 8/8/00Z (Fig. 9). One of the questions to be addressed in this section is: does the TC convection interact with the orographically induced convection constructively or destructively? One way to answer this question is to examine the orographic rain that occurred in the SW CMR. Moreover, we wanted to verify the orographic impact on the rainfall in NE and SW of the CMR. These two areas were considered because the typhoon made landfall around the NE part of CMR, and a massive amount of rainfall was recorded in the SW CMR. We used these two separate analyses for the periods 8/7/00Z – 8/8/00Z and 8/7/06Z – 8/8/06Z to examine the orographic rain generation and enhancement processes in NE and SW of the CMR, respectively. In both cases, the vertical cross-sections through NE (i, j) and SW (i', j') of the CMR were used to access how the heavy rainfall was generated and enhanced at the NE (Fig. 9) and SW (Fig. 12) of Taiwan's CMR. Fig. 10 shows the vertical cross-sections of vertical velocity and total water content along 24.3°N. At 8/7/00Z, the wind impinges on the windward side of the terrain and moves up due to orographic lifting and induces rainfall characterized by the total water content at the same location, and they both intensify progressively. Considering the location of the typhoon center (about 200 km), the rain produced at the windward side of the terrain does mostly appear to have been initiated by the terrain and not by the tropical cyclone (Fig. 9). Also, looking at the blue line contour in the vertical cross-section (Fig. 11), there was no rain at the far upstream location of the terrain. As one gets closer to the upslope, there is a gradual increase of rainfall, which can be largely credited to the orographic generation effect of the CMR.

Afterward, the rainfall was enhanced continuously, especially at the windward side of terrain with a rain rate of 70 mm/3 h, 149 mm/3 h, and 173 mm/3 h at 8/7/00Z, 8/7/06Z and 8/7/12Z respectively. The highest rainfall rate (265 mm/3 h) occurred on 8/7/18Z (red line), and six (6) hours later (8/8/00Z), declined to 239 mm/3 h (gray line)

Table 2
Testing of the modified Orographic Rain Index (ORI).

Event	V_n (m s^{-1})	Mountain Slope ($\partial h/\partial n$)	L_s ($\times 10^3$m)	c_s (m s^{-1})	(L_s/c_s) (s)	q_v (g kg^{-1})	ORI [V_n ($\partial h/\partial n$) (L_s/c_s) q_v]	Daily Rainfall (mm)
Value used for normalization[a]	20.0	0.030	100	5.0	20,000	20.0		
Hurricane Hugo (1989), USA	43.7	0.037	200	6.4	31,250	17.0	3.6	261
Hurricane Isabel (2003), USA	43.7	0.034	225	4.5	50,000	14.0	4.3	513
Supertyphoon Bilis (2000)	45.7	0.038	203	6.4	31,719	20.0	4.6	949
Typhoon Toraji (2001)	30.3	0.088	101	4.2	24,048	22.3	6.0	664
Typhoon Krosa (2007)	40.3	0.086	188	4.5	41,778	18.1	10.9	559
Typhoon Sepat (2007)	30.5	0.089	138	4.3	32,093	18.3	6.7	494
Typhoon Sinlaku (2008)	35.0	0.093	175	2.7	64,815	18.9	16.6	539
Typhoon Jangmi (2008)	57.3	0.078	120	5.0	24,000	17.7	7.9	568
Typhoon Fung-Wong (2008)	37.5	0.078	129	5.5	23,455	19.7	5.6	415
Typhoon Morakot (2009)	31.3	0.088	287	3.0	95,667	19.5	21.4	1402
Typhoon Fanapi (2010)	37.0	0.089	166	6.2	26,774	17.7	6.5	603
Typhoon Saola (2012)	33.3	0.078	111	5.4	20,556	18.7	4.2	212

[a] The values are normalized by those in the first row.

(Fig. 11). This enhancement can be related to the merging of orographic initiated rain and TC rain at 8/7/18Z (Fig. 10). Before the merging, between longitude 122.5E and 123.0E at 8/7/12Z, the total water content plot shows the typhoon's outer rainband approaching the windward side of the terrain and generating a maximum rainfall rate of 173 mm/3 h. Six hours (6 h) later, the initiated orographic rainfall merged with the TC rain at 8/7/18Z and caused the highest rainfall rate of 265 mm/3 h. One detail of significance is, during the enhancement period, the rain rate increased substantially from 173 mm/3 h to 265 mm/3 h, which is an increment of 92 mm/3 h. The rise in the rainfall rate is quite a bit higher than the rain rate increments of 79 mm/3 h and 42 mm/3 h between 8/7/00Z – 8/7/06Z, and 8/7/06Z – 8/7/12Z, respectively. In summary, the generation of typhoon Morakot's heavy orographic TC rain is mainly associated with the high and steep CMR of Taiwan. This means orographic lifting plays a major role in the generation of heavy orographic TC rainfall. For the maximum rainfall enhancement, it is largely related to the merging of orographic initiated rain and TC rain.

For the rainfall decrease, it is mainly due to the destruction of Morakot's structure when it impinged on the high CMR, evidenced by weakening convection at the upslope side of the CMR (Fig. 11). The vertical cross-section was kept constant at latitude 24.3°N in Fig. 11 because the cross-section line passed through the area where maximum rainfall occurred at the NE of the CMR. This means, the rainfall decrease was not a result of the shifting of rainfall maximum but mostly due to the weakening convection of the typhoon. Also, the weakening of convection is related to the strong orographic blocking effect, which caused the wind to flow around the topography instead of flow over the terrain. This is evidenced by the variation of maximum wind speed of 60 ms^{-1}, 70 ms^{-1}, 90 ms^{-1}, 70 ms^{-1}, and 40 ms^{-1} at 8/7/00Z, 8/7/06Z, 8/7/12Z, 8/7/18Z and 8/8/00Z, respectively. With the significant reduction in maximum wind speed from 70 ms^{-1} to 40 ms^{-1}, the blocking effect could be related to the reduction of Froude number (U/Nh) at 8/8/00Z. Hence, it did not have enough energy to overcome the terrain and resulted in a transition of "flow-over" to "flow-around" regime and led to upslope rainfall depletion (e.g., Chen and Lin, 2005).

Likewise, the vertical cross-section j was analyzed, and it was setup to follow the wind flow direction at NE of the CMR intending to examine the impact of the CMR on the wind flow (Fig. S1 in supplementary material). At 8/7/00Z, there is a strong updraft which coincides with large water vapor content at the windward side of the CMR. The CMR initiated this strong updraft and total water content before the typhoon impacted the CMR. The initiated convection increased in time, especially when the typhoon made landfall at 8/7/12Z. The merging of initiated convection by the CMR and typhoon associated convection could be the reason for the enhanced convection. The maximum rainfall location (Fig. 11) shifted eastward, and that caused a reduction in the upward vertical velocity and total water content from 8/7/18Z to 8/8/00Z (Fig. S1 in supplementary material). Moreover, the reduction is not related to the strong blocking effect because the terrain is not as steep as in the vertical cross-section in Fig. 10.

This finding encouraged us further to examine the mechanisms caused the intensification of rainfall at the SW of the CMR (Fig. 12). Fig. 13 shows the vertical cross-sections of vertical velocity and total water content from 8/7/06Z to 8/8/06Z that were used for the analysis. It is seen that strong vertical velocity with large water vapor content occurred at the upstream of the CMR, and the high and steep terrain generates this since the typhoon was about 150 km away, and the outer rainband had not impacted the SW of the CMR yet during 8/7/06Z. This implies that the southwest monsoonal current, which impinged on the

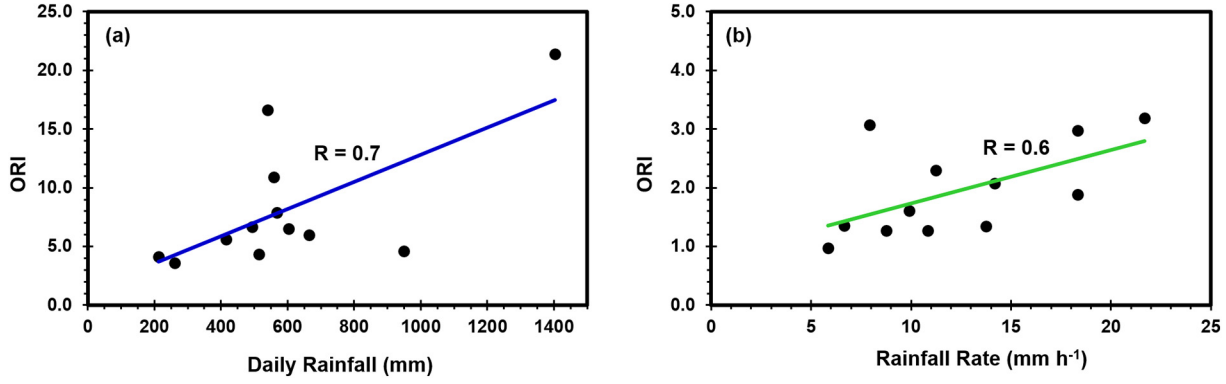

Fig. 8. The relationship between the modified ORI and daily rainfall (mm) of twelve (12) TC cases, including Typhoon Morakot (2009) with the highest ORI and rainfall of 21.4 and 1402 mm respectively. (b) The relationship between ORI and hourly rainfall rate in six (6) regions of local maximum rainfall each for hurricanes Hugo (1989) and Isabel (2003) (Adapted after Rostom, 2015).

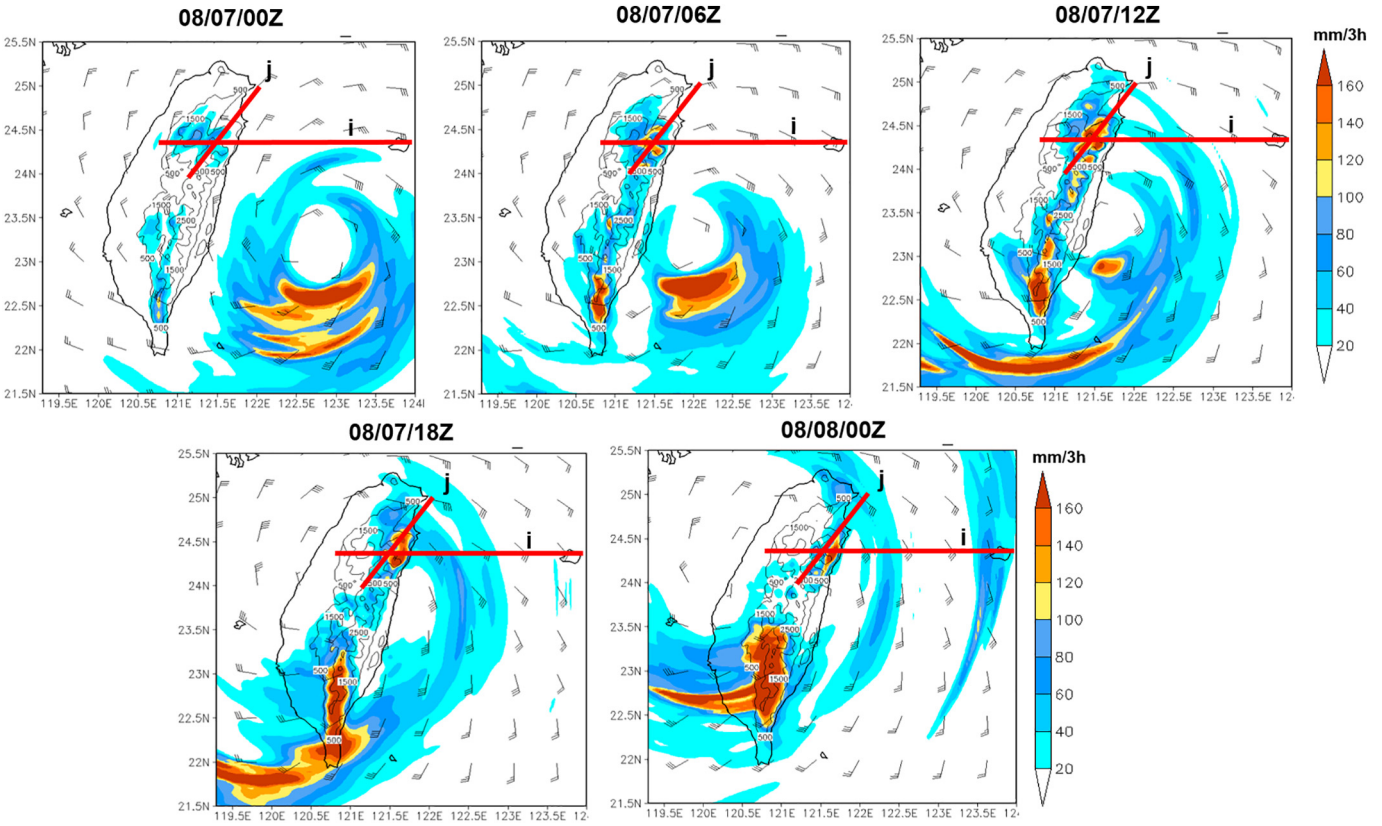

Fig. 9. Rain rate (shaded; mm/3 h) and vertical cross-section lines i (24.3°N) and j (diagonal) of WRF simulated Best case (E03) at the northeast of CMR during Typhoon Morakot's before and after landfall time (8/7/00Z – 8/8/00Z).

CMR, was orographically lifted, and it generated a reasonably large rain rate of about 106 mm/3 h on the upstream side of the terrain. On the lee side, it is characterized by gravity waves and downslope winds producing rain shadowing. This signifies that the effect of the CMR on the typhoon Morakot rainfall is orographically enhanced and suppressed on the upslope and lee slope of the terrain, respectively. The typhoon made landfall at 8/7/12Z, and a strong part of the outer rainbands passed in the South China Sea (Fig. 12). The vertical velocity and total water content continued increasing at the upstream side of the terrain, which is due to the arrival of the outer rainband impinging on the SW CMR and producing rain rate of about 147 mm/3 h. It is assumed this is the period the orographic initiated convection, and convection associated with the TC started to merge, as seen in Fig. 14. Later on, the typhoon moved northwest, followed by the outer rainbands moving polewards during 8/7/18Z. This shifted the maximum rainfall location northward and caused rainfall to be enhanced (202 mm/3 h) at the SW CMR, as seen in the purple contour line (Fig. 14). The merging continued during 8/8/00Z and gave a massive rain rate of about

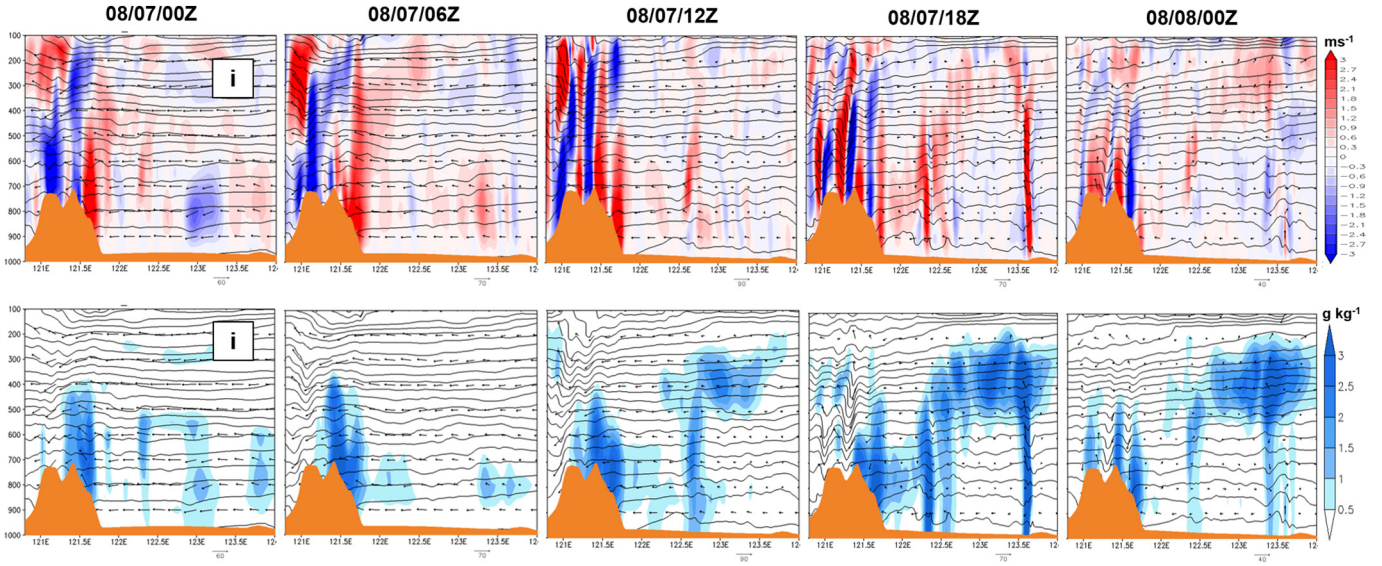

Fig. 10. Vertical cross-section of WRF simulated Best case (E03) at 24.3°N (line i) at the northeast of CMR for vertical velocity (ms^{-1}) and total water content ($g\ kg^{-1}$) (8/7/00Z – 8/8/00Z). The contour lines are isentropes from the surface to 100 hPa.

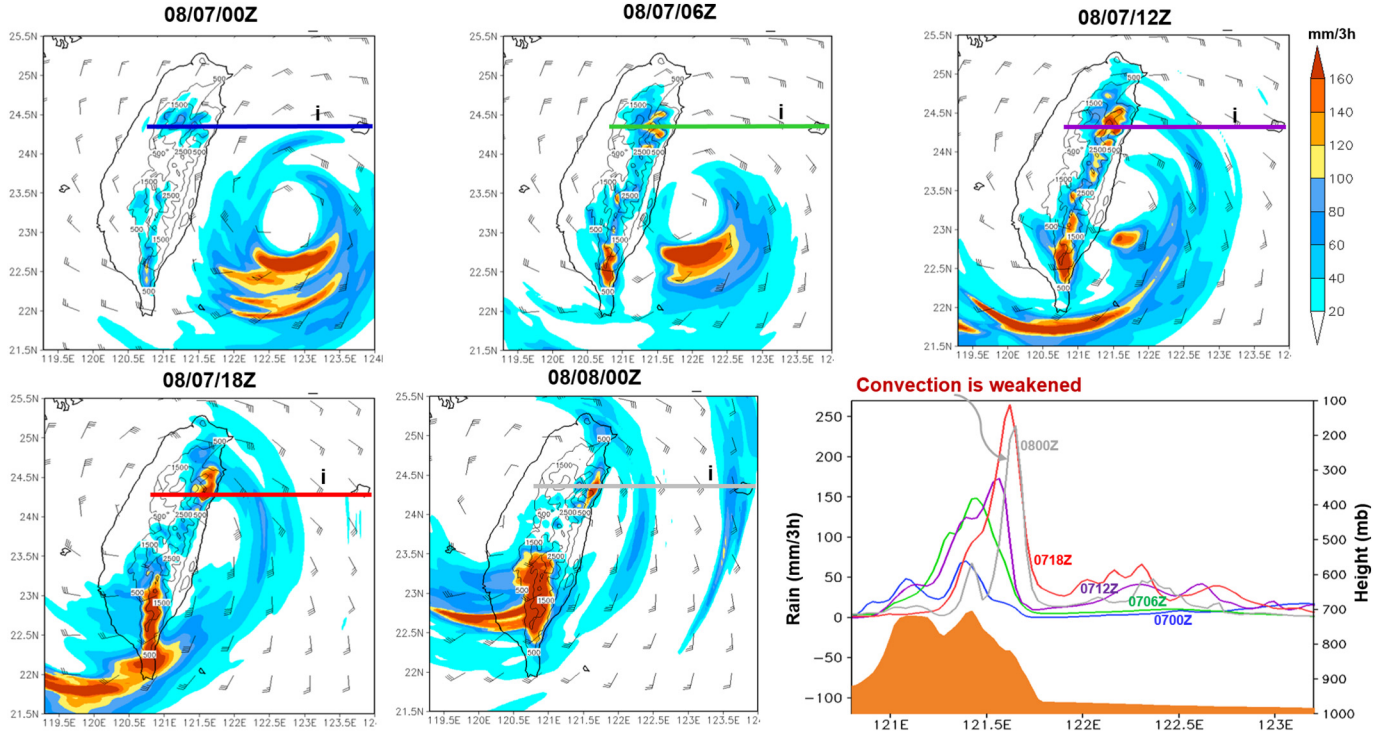

Fig. 11. Vertical cross-section of WRF simulated Best case (E03) at 24.3°N (line i) and the accumulated rainfall (shaded; mm/3 h) along the cross-section line (8/7/00Z – 8/8/00Z).

311 mm/3 h. Due to the shifting of the maximum rainfall location, the total water content and vertical velocity intensity decreased on 8/8/06Z and caused a suppressed rain rate of about 255 mm/3 h. This suggests that, at the SW CMR, the rainfall was reduced primarily due to the shifting of the maximum rainfall location and not strong blocking effect as in the NE CMR.

The vertical cross-section was varied to analyze whether the terrain blocking effect was a contributing factor in this reduction of rain rate

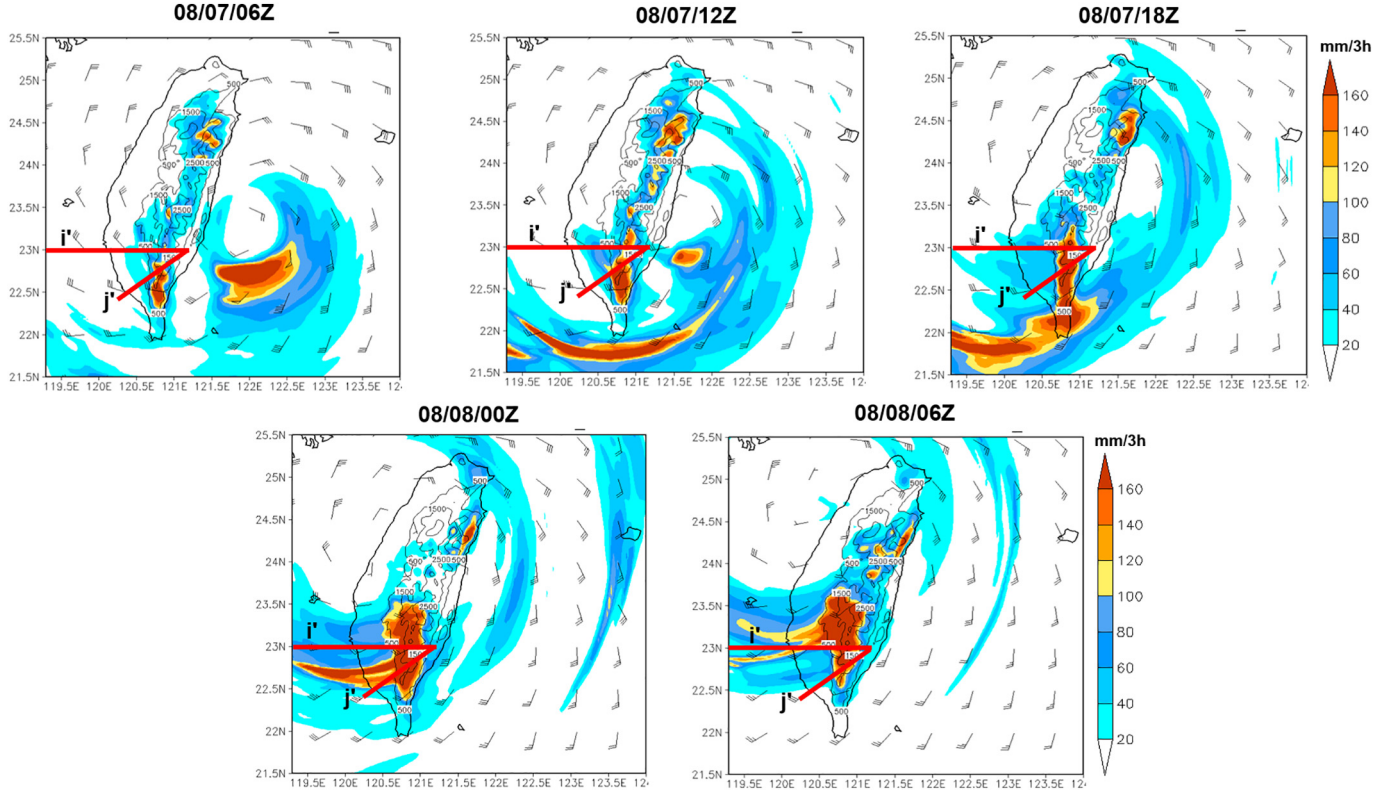

Fig. 12. Rain rate (shaded; mm/3 h) and vertical cross-section lines i' (23.0°N) and j' (diagonal) of WRF simulated Best case (E03) at the southwest of CMR during Typhoon Morakot's before and after landfall time (8/7/06Z – 8/8/06Z).

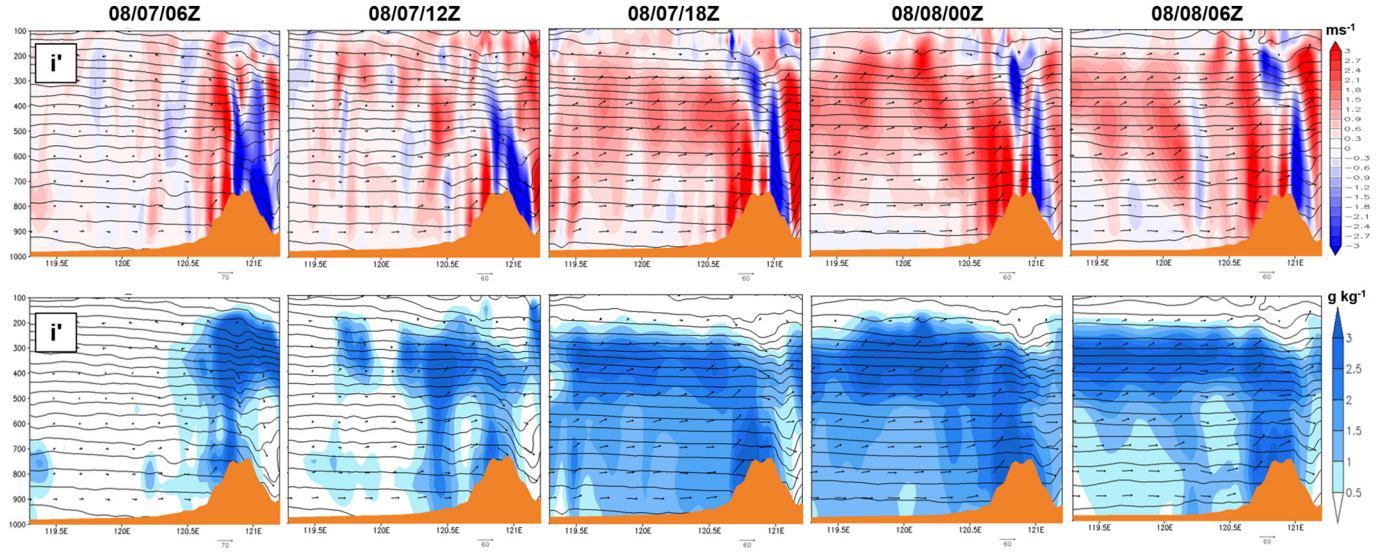

Fig. 13. Vertical cross-section of WRF simulated Best case (E03) at 23.0°N (line i') at the southwest of CMR for vertical velocity (ms^{-1}) and total water content ($g\ kg^{-1}$) (8/7/06Z – 8/8/06Z). The contour lines are isentropes from the surface to 100 hPa.

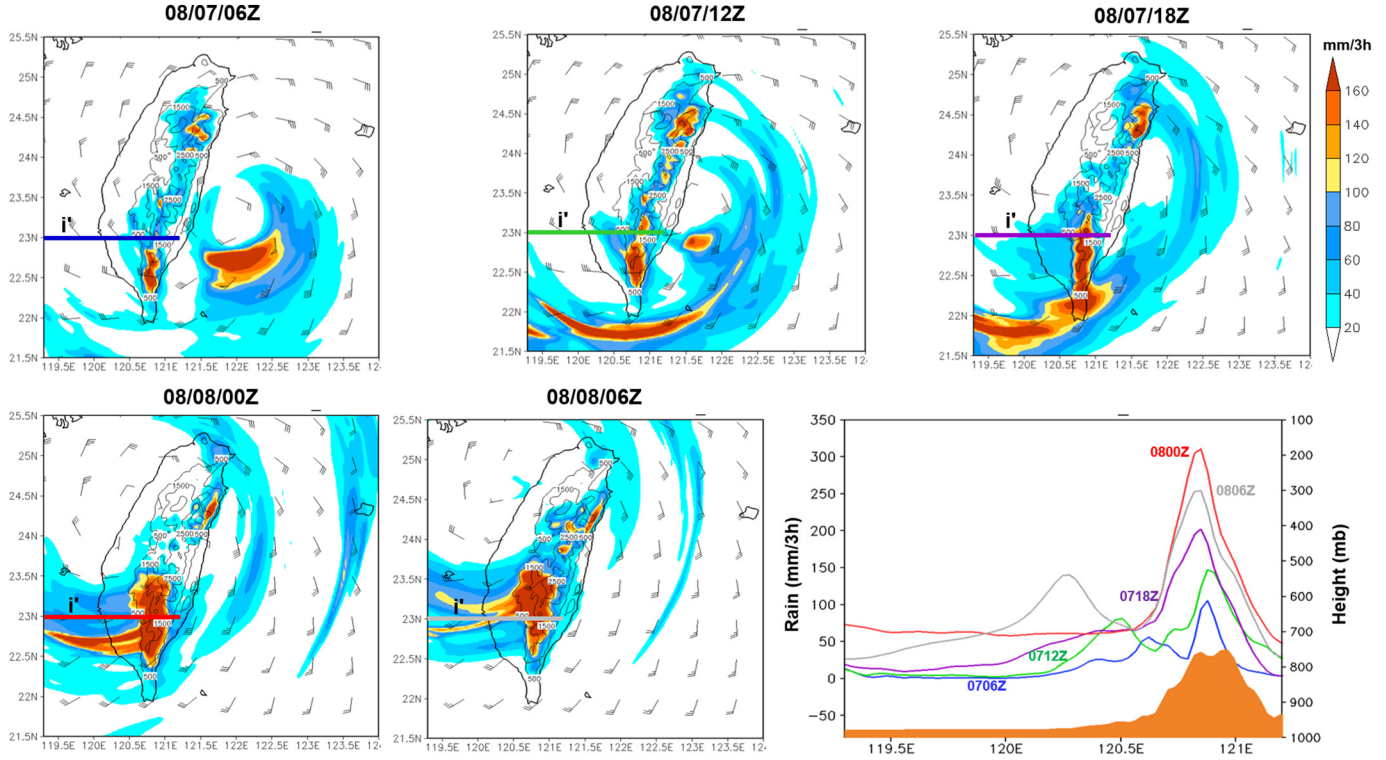

Fig. 14. Vertical cross-section of WRF simulated Best case (E03) at 23.0°N (line i') and the accumulated rainfall along the cross-section line (8/7/06Z – 8/8/06Z).

(Fig. 15). The cross-sections were adjusted to pass through the heaviest rainfall location at that time. From the line contours, the heaviest rainfall occurred on 8/7/12Z with rain rate of about 326 mm/3 h that was when the simulated typhoon made landfall. The heavy rainfall can be ascribed to the southwest monsoonal current and outer rainband, which merged into a very moist LLJ with preexisting convection. The outer rainband continued moving northward, and over a 12 h period (8/8/00Z), it gave rise to a second maximum rain rate of about 322 mm/3 h. Between longitude 119.5°E and 120°E, the red line contour shows a rise in rain rate, which is linked to the outer rainband (Fig. 15). As the typhoon moved northeast, it was followed by the northern movement of the rainfall maximum. This shows the terrain blocking effect was not the primary reason for the rainfall reduction in the SW CMR but instead due to the shifting of the maximum rainfall location.

Additionally, vertical velocity and total water content were examined using vertical cross-section diagonally (j') (Fig. S2 in supplementary material). At 8/7/06Z, there is a strong updraft at the windward side of the terrain, which continues to intensify from 8/7/12Z to 8/8/00Z until it declined on 8/8/06Z, which is related to the shifting of the maximum rainfall location, as explained above. This supports the idea of enhancement of orographic rainfall at windward, and dryness and rain shadow at the leeward side of the CMR. In summary, the above results have proven that TC convection interacted with the orographic

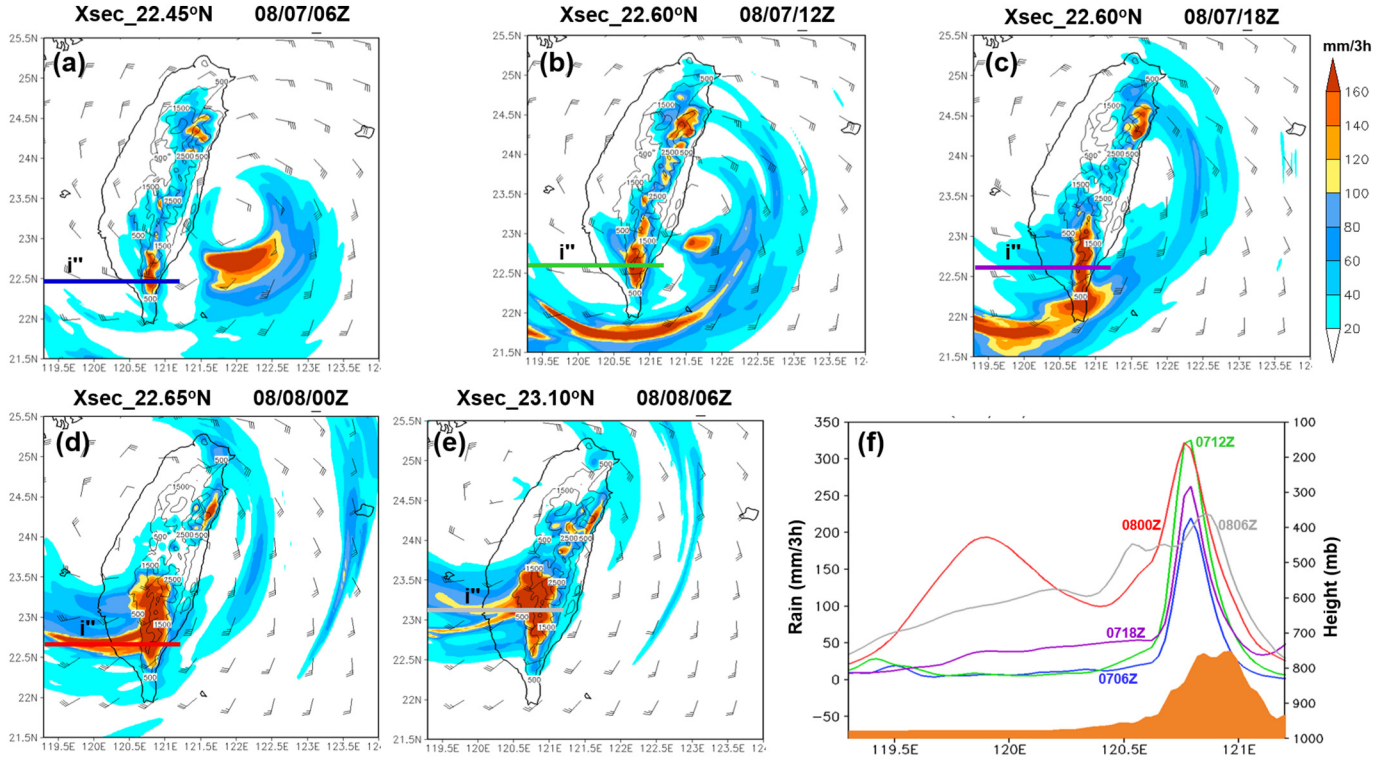

Fig. 15. Different vertical cross-sections of WRF simulated Best case (E03) at (a) 22.45°N (b, c) 22.60°N (d) 22.65°N (e) 23.10°N and (f) the accumulated rainfall (mm/3 h) along the cross-section lines (8/7/06Z – 8/8/06Z).

induced convection constructively in both the NE and SW of the CMR. Also, comparing the 24 h (8th – 9th LST) accumulated rainfall maximum, the Best case simulation outweighed the NT case by having 2024 mm of rainfall, and the NT case had 486 mm of rainfall (Fig. 5a). This implies orography plays an essential role in the enhancement of TC rainfall. Besides, we also compared the 3 h accumulated rainfall of the simulated Best case with the observed rainfall data from the Alishan weather station (23.30°N, 120.48°E) during the event of Typhoon Morakot (2009) (8/5/01Z – 8/9/22Z), as shown earlier in Fig. 5b.

5. Concluding remarks

In this study, we followed Lin's (2007) ingredient approach to examine more thoroughly the common ingredients for heavy orographic rain during the passage of Typhoon Morakot over the CMR. Then, based on these essential ingredients, we modified the Orographic Rain Index (ORI) proposed by Rostom (2015) and applied it to the Typhoon Morakot (2009), along with 11 other past typhoon and hurricanes, which produced heavy orographic rainfall. Finally, based on the essential ingredients and ORI, we explore the generation and enhancement mechanisms for extremely heavy rainfall, which occurred over the northeast and southwest of the Central Mountain Range (CMR) of Taiwan using the WRF model. A conceptual model summarizes these mechanisms responsible for orographic TC rain.

First, after a thorough examination of the common ingredients proposed by Lin et al. (2001), we found that the extreme rainfall associated with the passage of Morakot (2009) over the CMR was due to the essential orographic rain ingredients: high precipitation efficiency, strong low-level jet, steep terrain, large moisture upstream, large convective system, and slower movement of the typhoon. This was consistent with HL14, except there were more essential ingredients involved, such as high precipitation efficiency and a large convective system.

Second, we modified the Orographic Rain Index (ORI) proposed by Rostom (2015) by replacing the relative humidity (RH) with water vapor mixing ratio (q_v) to avoid the temperature dependency of RH, which led to ORI = $V_n\,(dh/dn)\,(L_s/c_s)\,q_v$. We then tested this modified ORI in twelve (12) TC cases, including Morakot, and was found to have a good correlation of 0.7 with daily rainfall (Fig. 8a), and also performed well in comparison with ORI estimated by Rostom (2015) (Fig. 8b). Thus, it can be used to help the prediction of extreme orographic TC rainfall.

Third, we investigated the mechanisms responsible for the extreme rainfall in the NE and SW of the CMR. From the analysis performed, we found the generation and enhancement of orographic rainfall were present in the NE and SW of the CMR. In the NE CMR, orographic rain was generated at the windward side of the terrain about 200 km before the typhoon impinged on the CMR. When the oncoming typhoon was approaching the CMR, the rainfall was enhanced gradually and continually by the CMR, producing rain rates of 70 mm/3 h, 149 mm/3 h, 173 mm/3 h at 8/7/00Z, 8/7/06Z and 8/7/12Z respectively. A maximum rain rate of 265 mm/3 h occurred on 8/7/18Z and 6 h later (8/8/00Z), the rain rate was depleted to 239 mm/3 h. The enhancement of orographic TC rain is associated with the merging of orographic initiated rain and TC rain. The rainfall declined primarily due to the destruction of Morakot's eyewall structure and weakening of its convection caused by the blocking effect of the high and steep CMR. The blocking effect is further indicated by the varying of the reduction of maximum wind flow speed from 70 ms^{-1} to 40 ms^{-1} during 8/7/18Z – 8/8/00Z. Comparing the wind speed, 8/8/00Z had a lower Froude number and consequently less energy to overcome the terrain and resulted in a transition of “flow-over” to “flow-around” regime, causing rainfall suppression.

For the SW CMR, orographic rain was generated by the southwesterly monsoonal current impinging on the southern CMR. The northwest rainband moved in while the typhoon approached NE of the CMR, then, the SW monsoonal current and the NW rainband merged into a very moist LLJ with preexisting convection. The merging of the orographic rain and the TC rain led to an extreme maximum rainfall rate of 311 mm/3 h starting at 8/8/00Z. This is illustrated in the

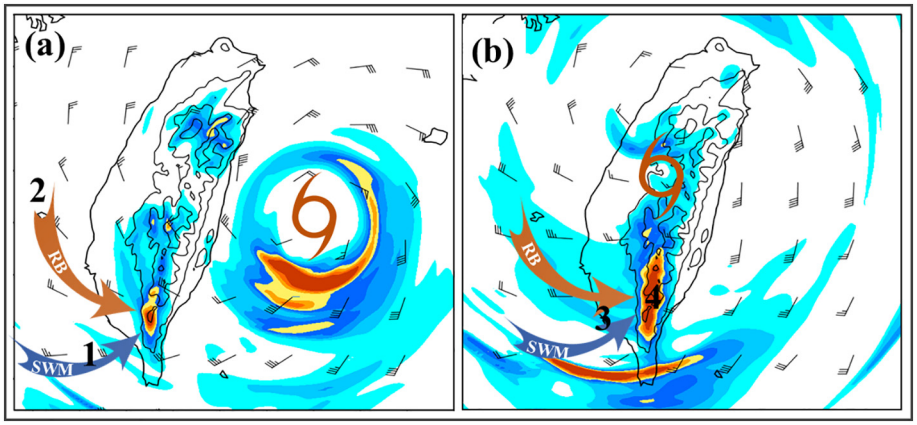

Fig. 16. A conceptual model showing four key processes associated with the generation and enhancement of orographic TC rain over the southwest of CMR during the passage of typhoon Morakot (2009): (1) Southwest monsoonal (SWM) current initiated orographic rainfall. (2) Northwest rainband (RB) moved in while typhoon approached the northeast of CMR. (3) Southwest monsoonal current and northwest rainband merged into a very moist LLJ with preexisting convection. (4) Orographic rain and TC rain merged and led to enhanced convection, which produced extreme rainfall.

conceptual model (Fig. 16). Afterward, this region of enhanced orographic TC rain moved northward along the western flank of the CMR and resulted in a rainfall rate reducing to 225 mm/3 h at that location. Comparatively, orographically initiated convection in the SW CMR was able to develop further and produced heavier rainfall than in the NE CMR. This clarifies that the increase of moist, unstable airflow associated with the TC rainband impinging on the SW CMR's steep terrain possesses enough key ingredients for producing heavy rainfall. Also, strong downslope winds and gravity waves help cut off rainfall on the lee slope both in the NE and SW of the CMR, which concludes that the effect of the CMR on the typhoon Morakot rainfall is the overwhelmingly orographic enhancement and suppression on the windward and leeward side of the terrain, respectively. Moreover, we have proven that TC convection interacted with the orographic induced convection constructively in both the NE and SW of the CMR.

Finally, unlike previous studies (e.g., Witcraft et al., 2005), CAPE played an essential role in producing heavy TC rain. Also, several other studies (e.g., Molinari and Vollaro, 2010) have shown that when it comes to tropical cyclones, the CAPE is strongly related to both the structure of the cyclone and the ambient vertical shear (CAPE in strongly sheared storms is for instance 60% larger downshear). Thus, ORI may be further modified to include the CAPE, so that it will be more inclusive. Also, apart from the enhancement of orographic rain, Taiwan's CMR initiated the rainfall, and this will require further analysis to investigate the relationship between terrain effect and high rainfall production in a non-TC environment. In other words, without a TC, which mechanisms can aid in producing heavy orographic rainfall? Further studies are needed since this can improve the forecasting accuracy of extreme orographic TC rain.

Declaration of Competing Interest

The authors declare that they have no known competing financial interests or personal relationships that could have appeared to influence the work reported in this paper.

Acknowledgments

The authors would like to acknowledge Drs. J. Zhang, A. Mekonnen, and L. Liu at North Carolina A&T State University for their insightful discussions and comments on this paper. In addition, editing of the manuscript made by Dr. M. Kaplan and remarks made by anonymous reviewers are highly appreciated. This research was supported by the National Science Foundation Award AGS-1265783 and National Center for Atmospheric Research (NCAR) Diversity Fund. The authors would like to acknowledge NCAR and Computational and Information Systems Laboratory (CISL) for their support of computing time on the Cheyenne supercomputer (Project No. UNCS0030).

Appendix A. Supplementary data

Supplementary data to this article can be found online at https://doi.org/10.1016/j.atmosres.2020.105160.

References

AMS, 2020. "LLJ". Glossary of Meteorology. American Meteorological Society Available at: http://glossary.ametsoc.org/wiki/"LLJ".
Chang, S.W.-J., 1982. The orographic effects induced by an island mountain range on propagating tropical cyclones. Mon. Weather Rev. 110, 1255–1270.
Chen, S.-H., Lin, Y.-L., 2005. Orographic effects on a conditionally unstable flow over an idealized three-dimensional mesoscale mountain. Meteorog. Atmos. Phys. 88, 1–21. https://doi.org/10.1007/s00703-003-0047-6.
Chiao, S., Lin, Y.-L., 2003. Numerical modeling of an orographically enhanced precipitation event associated with tropical storm Rachel over Taiwan. Weather Forecast. 18, 325–344. https://doi.org/10.1175/1520-0434(2003)018<0325:NMOAOE>2.0.CO;2.
Chien, F.-C., Kuo, H.-C., 2011. On the extreme rainfall of Typhoon Morakot (2009). J. Geophys. Res. Atmos. 116, 1–22. https://doi.org/10.1029/2010JD015092.
Doswell, C., Brooks, H., Maddox, R., 1996. Flash flood forecasting: an ingredients-based methodology. Weather Forecast. 11, 560–581.
Dudhia, J., 1989. Numerical study of convection observed during the Winter Monsoon Experiment using a mesoscale two-dimensional model. J. Atmos. Sci. 46, 3077–3107. https://doi.org/10.1175/1520-0469(1989)046<3077:NSOCOD>2.0.CO;2.
Frankhauser, J.C., 1988. Estimate of thunderstorm precipitation efficiency from field experiments in CCOPE. Mon. Wea. Rev. 116, 663–684.
FWM, 2019. Taiwan Physical Map. Free World Map. https://www.freeworldmaps.net/asia/taiwan/map.html.
Ge, X., Li, T., Zhang, S., Peng, M., 2010. What causes the extremely heavy rainfall in Taiwan during Typhoon Morakot (2009)? Atmos. Sci. Lett. 11, 46–50. https://doi.org/10.1002/asl.255.
Hong, S.-Y., Noh, Y., Dudhia, J., 2006. A new vertical diffusion package with an explicit treatment of entrainment processes. Mon. Weather Rev. 134, 2318–2341. https://doi.org/10.1175/MWR3199.1.
Hong, C.-C., Lee, M.-Y., Hsu, H.-H., Kuo, J.-L., 2010. Role of submonthly disturbance and 40-50 day ISO on the extreme rainfall event associated with Typhoon Morakot (2009) in Southern Taiwan. Geophys. Res. Lett. 37, 1–6. https://doi.org/10.1029/2010GL042761.
Huang, Y.-C., Lin, Y.-L., 2014. A study on the structure and precipitation of Morakot (2009) induced by the Central Mountain Range of Taiwan. Meteorog. Atmos. Phys. 123, 115–141. https://doi.org/10.1007/s00703-013-0290-4. (HL14).
Kain, J.S., 2004. The Kain - Fritsch convective parameterization: an update. J. Appl. Meteorol. 43, 170–181. https://doi.org/10.1175/1520-0450(2004)043<0170:TKCPAU>2.0.CO;2.
Lin, Y.-L., 1993. Orographic effects on systems over Taiwan. Terr. Atmos. Ocean. Sci. 4, 381–420.
Lin, Y.-L., 2007. Mesoscale Dynamics. Cambridge University Presshttps://doi.org/10.1017/CBO9780511619649.
Lin, Y.-L., Farley, R.D., Orville, H.D., 1983. Bulk parameterization of the snow field in a cloud model. J. Clim. Appl. Meteorol. 22, 1065–1092. https://doi.org/10.1175/1520-0450(1983)022<1065:BPOTSF>2.0.CO;2.
Lin, Y.-L., Chiao, S., Wang, T.-A., Kaplan, M.L., Weglarz, R.P., 2001. Some common ingredients for heavy orographic rainfall. Weather Forecast. 16, 633–660. https://doi.org/10.1175/1520-0434(2001)016<0633:SCIFHO>2.0.CO;2.
Lin, Y.-L., Chen, S.-Y., Hill, C.M., 2005. Control parameters for the influence of a Mesoscale Mountain Range on cyclone track continuity and deflection. J. Atmos. Sci. 62, 1849–1866.
Lin, C.-Y., Hsu, H.-M., Sheng, Y.-F., Kuo, C.-H., Liou, Y.-A., 2011. Mesoscale processes for super heavy rainfall of typhoon Morakot (2009) over southern Taiwan. Atmos. Chem. Phys. 11, 345–361. https://doi.org/10.5194/acp-11-345-2011.

Lin, Y.-L., Chen, S.-H., Liu, L., 2016. Orographic influence on basic flow and cyclone circulation and their impacts on track deflection of an idealized tropical cyclone. J. Atmos. Sci. 73, 3951–3974. https://doi.org/10.1175/JAS-D-15-0252.1.

Mlawer, E.J., Taubman, S.J., Brown, P.D., Iacono, M.J., Clough, S.A., 1997. Radiative transfer for inhomogeneous atmospheres: RRTM, a validated correlated-k model for the longwave. J. Geophys. Res. D Atmos. 102, 16663–16682. https://doi.org/10.1029/97jd00237.

Molinari, J., Vollaro, D., 2010. Distribution of helicity, CAPE, and shear in tropical cyclones. J. Atmos. Sci. 67, 274–284. https://doi.org/10.1175/2009JAS3090.1.

NASA - Hurricane Season, 2009. Morakot (Western Pacific) [WWW Document], 2009. https://www.nasa.gov/mission_pages/hurricanes/archives/2009/h2009_Morakot.html (accessed 12.3.19).

Nguyen, H.V., Chen, Y.-L., 2011. High resolution initialization and simulations of Typhoon Morakot (2009). Mon. Weather Rev. 139, 1463–1491.

Purnell, D.J., Kirshbaum, D.J., 2018. Synoptic control over orographic precipitation distributions during the Olympics Mountains Experiment (OLYMPEX). Mon. Weather Rev. 146, 1023–1044. https://doi.org/10.1175/MWR-D-17-0267.1.

Rostom, R., 2015. Effects of Orography on Track Continuity of Cyclones and Precipitation Associated with Tropical Cyclones Passing over the Southern-Central Appalachian Mountains. Ph.D. Diss., North Carolina Agricultural and Technical State University. http://ncat.idm.oclc.org/login?url=https://search.proquest.com/docview/1695272765?accountid=12711.

Skamarock, W.C., Klemp, J.B., Dudhi, J., Gill, D.O., Barker, D.M., Duda, M.G., Huang, X.-Y., Wang, W., Powers, J.G., 2008. A Description of the Advanced Research WRF Version 3. Technical Report. https://doi.org/10.5065/D6DZ069T.

Staff, W., 2009. TAIWAN Billions Allocated for Reconstruction in Wake of Typhoon Morakot [WWW Document]. http://www.asianews.it/index.php?l=en&art=16097&size=A.

Tao, W.-K., Simpson, J., McCumber, M., 1989. An ice-water saturation adjustment. Mon. Weather Rev. 117, 231–235. https://doi.org/10.1175/1520-0493(1989)117<0231:aiwsa>2.0.co;2.

Tao, W., Shi, J., Lin, P., 2011. High-resolution numerical simulation of the extreme rainfall associated with Typhoon Morakot. Part I: comparing the impact of microphysics and PBL parameterizations. Terr. Atmos. Ocean. Sci. 22, 673–696. https://doi.org/10.3319/TAO.2011.08.26.01(TM)1.

Typhoon, Digital, 2019. Typhoon 200908 (Morakot) – General Information (Pressure and Track Charts). Japan Meteorological Agency. http://agora.ex.nii.ac.jp/digital-typhoon/summary/wnp/s/200908.html.en.

Wang, S.-T., 1980. Prediction of the behavior and strength of typhoons in Taiwan and its vicinity. In: Res. Rep. 18, Natl. Sci. Counc. Taipei, Taiwan.

Witcraft, N.C., Lin, Y.-L., Kuo, Y.-H., 2005. Dynamics of orographic rain associated with the passage of a tropical cyclone over a mesoscale mountain. Terr. Atmos. Ocean. Sci. 16, 1133–1161.

Wu, C.-C., 2013. Typhoon Morakot: Key findings from the journal TAO for improving prediction of extreme rains at landfall. Bull. Am. Meteorol. Soc. 94, 155–160. https://doi.org/10.1175/BAMS-D-11-00155.1.

Wu, L., Liang, J., Wu, C.-C., 2011. Monsoonal influence on Typhoon Morakot (2009). Part I: Observational analysis. J. Atmos. Sci. 68, 2208–2221. https://doi.org/10.1175/2011JAS3730.1.

Xie, B., Zhang, F., 2012. Impacts of typhoon track and Island topography on the heavy rainfalls in Taiwan associated with Morakot (2009). Mon. Weather Rev. 140, 3379–3394. https://doi.org/10.1175/MWR-D-11-00240.1.

Yang, M.-J., Ching, L., 2005. A modeling study of Typhoon Toraji (2001): Physical parameterization sensitivity and topographic effect. Terr. Atmos. Ocean. Sci. 16, 177–213. https://doi.org/10.3319/TAO.2005.16.1.177(A).

Yang, M.-J., Zhang, D.-L., Huang, H.-L., 2008. A modeling study of Typhoon Nari (2001) at landfall. Part I: Topographic effects. J. Atmos. Sci. 65, 3095–3115. https://doi.org/10.1175/2008JAS2453.1.

Yen, T.-H., Wu, C.-C., Lien, G.-Y., 2011. Rainfall simulations of Typhoon Morakot with controlled translation speed based on EnKF data assimilation. Terr. Atmos. Ocean. Sci. 22, 647–660. https://doi.org/10.3319/TAO.2011.07.05.01(TM).

Yu, C.-K., Cheng, L.-W., 2013. Distribution and mechanisms of orographic precipitation associated with typhoon Morakot (2009). J. Atmos. Sci. 70, 2894–2915. https://doi.org/10.1175/JAS-D-12-0340.1.